

**МЕХАНОАКТИВИРОВАННЫЕ КОМПОЗИТЫ НА ОСНОВЕ ДИСУЛЬФИДА ВОЛЬФРАМА:
СИНТЕЗ И СВОЙСТВА****Ал.С. Акимов, Н.А. Жиров, Е.А. Сударев, А.С. Акимов**

Альберт Софронович Акимов (ORCID 0000-0003-3567-8148)*, Никита Алексеевич Жиров (ORCID 0000-0002-9165-6851), Аким Семенович Акимов (ORCID 0000-0001-7953-1477)

Лаборатория каталитических превращений легких углеводородов, Институт химии нефти СО РАН, пр. Академический, 4, Томск, Российская Федерация, 634055

E-mail: albertus98@mail.ru*, krigsnu@mail.ru, zerobox70@mail.ru

Евгений Александрович Сударев (ORCID 0000-0002-5596-4048)

Национальный исследовательский Томский политехнический университет, пр. Ленина, 30, Томск, Российская Федерация, 634034

E-mail: sudarev@tpu.ru

В данной работе исследованы физико-химические свойства механоактивированных композитов (далее по тексту механокомпозитов), полученных при механической активации коммерческого порошка дисульфида вольфрама в планетарной мельнице. Механоактивация проводилась в течение 2, 4 и 8 ч, однако в данной работе представлены результаты для последних двух экспериментов. Ускорение мелющих тел контролировалось через регулировку частоты, значение частоты в 15,5 Гц, согласно расчетам, соответствует ускорению мелющих тел в 50 м/с² или 5G. Материал, из которого изготовлены размольные шары – нержавеющая сталь. Из-за относительно малых значений ускорения, загрязнения образца компонентами нержавеющей стали в результате эрозии поверхности, возникающей при соударении шаров между собой и со стенками размольного стакана, не происходит. Механоактивация проводилась в инертной среде аргона, поскольку это были предварительные исследования, и поэтому была необходимость максимального сокращения учитываемых параметров среды. Тем не менее, процесс окисления будет происходить в процессе выгрузки образца из размольного стакана планетарной мельницы. Полученные механокомпозиты являются предшественниками для синтеза монокомпонентных катализаторов для переработки тяжелого нефтяного остатка. Для этой цели необходимо получение механокомпозитов, содержащих в своем составе триоксид вольфрама, а также дисульфид вольфрама. Представлены результаты влияния продолжительности механоактивации и поверхностно активных добавок на свойства полученных механокомпозитов. Полученные соединения охарактеризованы методами рентгенофазового анализа (РФА), ИК-спектроскопии, сканирующей электронной микроскопии (СЭМ, термогравиметрии (ТГ), синхронного термического анализа (СТА).

Ключевые слова: механическая активация, дисульфид вольфрама, механокомпозит

Для цитирования:

Акимов Ал.С., Жиров Н.А., Сударев Е.А., Акимов А.С. Механоактивированные композиты на основе дисульфида вольфрама: синтез и свойства. *Изв. вузов. Химия и хим. технология.* 2024. Т. 67. Вып. 8. С. 36–43. DOI: 10.6060/ivkkt.20246708.2t.

For citation:

Akimov Al.S., Zhiron N.A., Sudarev E.A., Akimov A.S. The mechanically activated composites based on tungsten disulfide: synthesis and properties. *ChemChemTech [Izv. Vyssh. Uchebn. Zaved. Khim. Khim. Tekhnol.]*. 2024. V. 67. N 8. P. 36–43. DOI: 10.6060/ivkkt.20246708.2t.

THE MECHANICALLY ACTIVATED COMPOSITES BASED ON TUNGSTEN DISULFIDE: SYNTHESIS AND PROPERTIES

A.I.S. Akimov, N.A. Zhiron, E.A. Sudarev, A.S. Akimov

Albert S. Akimov (ORCID 0000-0003-3567-8148)*, Akim S. Akimov (ORCID 0000-0001-7953-1477), Nikita A. Zhiron (ORCID 0000-0002-9165-6851)

Laboratory of Catalytic Transformations of Light Hydrocarbons, Institute of Petroleum Chemistry, Siberian Branch of the RAS, Akademicheskii ave., 4, Tomsk, 413100, Russia
E-mail: albertus98@mail.ru*, krigsnu@mail.ru, zerobox70@mail.ru

Evgeny A. Sudarev (ORCID 0000-0002-5596-4048)

National Research Tomsk Polytechnic University, Lenina ave., 30, Tomsk, 634034, Russia
E-mail: sudarev@tpu.ru

In this work, the physicochemical properties of mechano-activated composites (hereinafter referred to as the mechanocomposites) obtained by mechanical activation of commercial tungsten disulfide powder in a planetary mill were studied. Mechanical activation was carried out for 2, 4 and 8 h, but this work presents the results for the last two experiments. The acceleration of the grinding media was controlled through frequency adjustment; a frequency value of 15.5 Hz, according to calculations, corresponds to an acceleration of the grinding media of 50 m/s² or 5G. The material of the balls from which the grinding balls are made is stainless steel. Due to the relatively low acceleration values, the problem of contamination of the sample with stainless steel components does not occur as a result of surface erosion that occurs when the balls collide with each other and with the walls of the grinding bowl. Mechanical activation was carried out in an inert argon environment, since these were preliminary studies and therefore there was a need to minimize the environmental parameters taken into account. However, the oxidation process will occur during the process of discharging the sample from the grinding bowl of the planetary mill. The resulting mechanocomposites are precursors for the synthesis of monocomponent catalysts for the processing of heavy oil residue. For this purpose, it is necessary to obtain mechanocomposites containing tungsten trioxide and tungsten disulfide. The results of an experimental study of the influence, mainly, of the duration of mechanical activation on the production of tungsten mechanocomposites are presented. The resulting compounds were characterized by X-ray phase analysis (XRD), IR spectroscopy, scanning electron microscopy (SEM), thermogravimetry (TGA) and simultaneous thermal analysis (STA).

Keywords: mechanical activation, tungsten disulfide, mechanocomposite

INTRODUCTION

Tungsten disulfide (WS₂) is a 2D material from the class of transition metal dichalcogenides. They are anisotropic materials with strong intra-layer bonding and weak inter-layer interactions. It is known that tungsten disulfide is used as an active component of oil refining catalysts, as well as in the production of photoconductors, as lubricants, impact-resistant composites, etc. [1-5].

Currently, researchers are paying much attention to composites, particularly tungsten disulfide and tungsten oxide (WS₂/WO₃ or WS₂-WO₃). Due to the synergistic effect inherent in such composites, the efficiency of the positive properties will be higher than when these components are used separately [6].

Thus, the analysis of literature data in the field of oil refining has shown that to obtain lighter and higher quality fractions from heavy hydrocarbon feedstock (heavy oils, residual fractions) use transition metals or their compounds (sulfides and oxides), in particular, tungsten and its derivatives.

At the same time, solid-phase processes initiated by mechanical action are currently becoming the subject of intensive research. Mechanochemical synthesis in a high-energy ball mill is a rapidly developing waste-free technology, which opens wide prospects in the field of obtaining new modern materials and composites for various purposes - for example, catalytic systems. The principle of mechanochemical processing is based on the conversion of mechanical en-

ergy into chemical energy, which increases the reactivity and induces a wide range of solid-state chemical reactions.

EXPERIMENTAL TECHNIQUE

Mechanical activation of tungsten disulfide powder (“Reakhim”) was carried out in a planetary mill under the following conditions: duration of mechanical activation 2, 4 and 8 h, medium - argon, acceleration of grinding bodies 50 m/s^2 ($\sim 5\text{G}$), ball material - stainless steel, mass ratio sample:grinding elements - 1:72.

To study using Fourier transform infrared spectroscopy (Nicolet 5700 from Thermo Fisher Scientific), samples were pressed into disks with spectrally pure KBr. The weights of the substance and matrix were constant, each spectrum was obtained as a result of 64 scans in the range of $400\text{--}4000 \text{ cm}^{-1}$ with a resolution of 4 cm^{-1} .

X-ray diffraction (XRD) was carried out on a D8 Advance powder diffractometer equipped with a Lynx-Eye one-dimensional detector and a $\text{K}\beta$ filter with $\text{CuK}\alpha$ radiation. The shooting was carried out in the angle range $10^\circ < 2\theta < 86^\circ$. The structural parameters were refined using powder diffraction patterns using the Rietveld method using Topas 4.2 software.

The morphology of the samples was studied on a JCM-6000 microscope at an accelerating voltage of 15 kV.

Complex thermal analysis was carried out using a synchronous thermal analyser STA 449C Jupiter (NETZSCH) combining simultaneous measurement of mass changes (thermogravimetry) and heat fluxes (differential scanning calorimetry), combined with a quadrupole mass spectrometer QMS 403 C Aeolos (NETZSCH) to analyse gases released during heating of the sample. The sample was heated from a temperature of $50 \text{ }^\circ\text{C}$ to $750 \text{ }^\circ\text{C}$ at a rate of $15 \text{ }^\circ\text{C}/\text{min}$ in a dynamic air atmosphere (gas flow rate of $30 \text{ ml}/\text{min}$).

RESULTS AND DISCUSSION

The XRD of the obtained mechanocomposites at different duration of the mechanoactivation process was compared. For all processes conditions were the same: temperature - $350 \text{ }^\circ\text{C}$, medium - argon, surfactant - ethanol; acceleration of grinding bodies - 5 G ($\sim 50 \text{ m/s}^2$), ball material - steel, ball/compound mass ratio - 1:72.

The initial tungsten disulfide as a comparison sample and mechanically activated tungsten disulfides after 4 and 8 h of mechanoactivation were selected. Fig. 1 demonstrates the comparison of the obtained diffractograms:

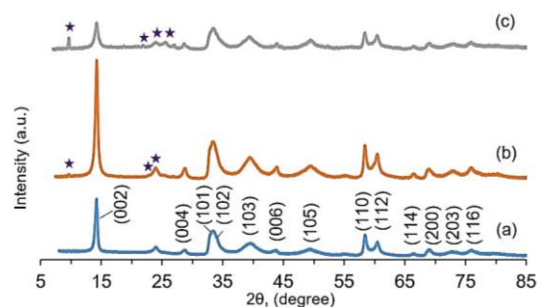


Fig. 1. Comparison of X-ray diffraction patterns: (a) raw WS_2 , (b) sample M-1, (c) sample M-2 – obtained mechanocomposites after 4 and 8 h, respectively W_xO_y reflexes are represented as *

Рис. 1. Сравнение рентгеновских дифрактограмм: а) исходного дисульфида (WS_2), б) образца М-1, с) образца М-2 – полученные механокомпозиты после 4 и 8 ч, соответственно. Рефлексы W_xO_y представлены как *

According to the results of the obtained X-ray diffraction patterns, it can be concluded that the powders of mechanocomposite based on tungsten oxide and tungsten disulfide consist of well-formed crystalline phases. Presumably, this indicates that despite the increase in the dispersibility of individual crystallites due to mechanical action under mechanical activation conditions, a significant number of unamortised phases remain in general. The obtained profile of the initial tungsten disulfide powder shows high-intensity narrow peaks corresponding to the positions of hexagonal WS_2 . In addition, low intensity reflections characteristic of tungsten oxides are also present in the initial disulfide. After ball milling, both the appearance of the reflex at 12° , [7-12] related to the tungsten trioxide phases, and an increase in the intensity of the other reflexes associated with the trioxides are observed, as shown in Fig. 1 (M-1 and M-2). A slight broadening of the reflex (002) indicates a decrease in the degree of packing [13]. In contrast to vibrating mills and stirred media mills [14], a high-energy planetary mill at a grinding acceleration value equal to 5G can generate a significant breaking stress, resulting in a reduction in size along the basal plane, which can be detected by the broadening of peak (110).

At 14° , a high-intensity reflex characteristic of tungsten disulfide phases is observed in the (002) plane. Intense reflexes are also observed at 23.4° , 33.8° , 44° , 50° , 58° and 61° , belonging to the WO_3 phases. A low-intensity reflex at 12° also belongs to the tungsten trioxide phase. This indicates that the mechanoactivation for 4 h is insufficient to obtain the required amount of oxide phases, but the duration of 8 h contributes to a significant growth of tungsten oxide phases. Apparently, this is due to a fairly significant increase in the dispersibility of tungsten disulfide. Also at longer duration of mechanical activation more internal energy is

accumulated, that in pair with increase of dispersity contribute to more intensive initiation of oxidation in the process of transition from inert medium to air medium.

Diffractograms of M-1 and M-2 almost completely coincide with each other, no lateral shifts are observed. The intensities of characteristic bands almost completely coincide. The reflexes at higher angles 2θ for MS-2 are slightly more intense than for M-1 - the values diverge on average by about 15%, this may be due to the error of the measurement method.

Fig. 2 shows a comparison of X-ray diffraction patterns of the obtained mechanocomposites when varying the nature of the added surfactant. All X-ray diffraction patterns have a similar profile, the difference is only in the intensity of the reflex on the (001) plane at 14° . Compared to the original molybdenum disulfide without surfactant (M-1), the addition of different surfactants decreases the intensity of this plane, which presumably indicates that molybdenum disulfide is more consumed in reactions for the formation of molybdenum compounds, mainly represented by molybdenum oxides (M2-M5). However, on the other hand, there is no significant difference between the effect of surfactants on increasing the reactivity of molybdenum disulfide during the mechanoactivation process. Since the mechanoactivation is not carried out in solution, but using small amounts of surfactants, there are no problems of their removal from the system. Thus, when choosing the nature of surfactant should be guided by availability and economic feasibility, the most suitable to such criteria of the proposed compound is distilled water.

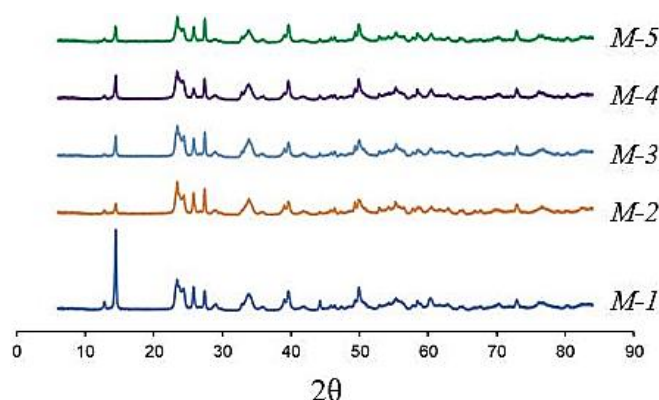


Fig. 2. Comparison of X-ray diffraction patterns of the obtained mechanocomposites with varying the nature of surfactant: M-1 - mechanocomposite without surfactant; M-2 - with ethanol; M-3 - with water; M-4 - with hexane; M-5 - with hexadecane
Рис. 2. Сравнение рентгенограмм полученных механокомпози- тов с варьированием природы ПАВ: М-1 – механокомпозит без ПАВ; М-2 – с этанолом; М-3 – с водой; М-4 – с гексаном; М-5 – с гексадеканом

To obtain more detailed information about the phases present, it is necessary to compare the data obtained in XRD with the results of thermal methods.

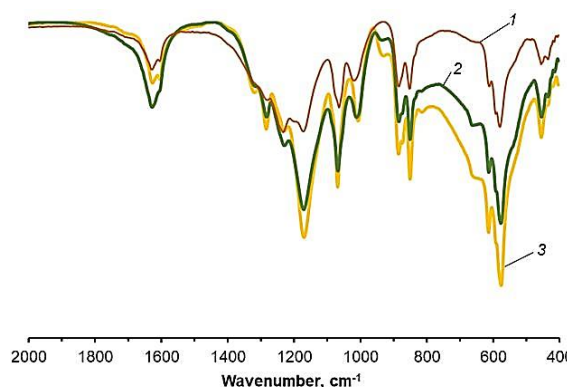


Fig. 3. Region of the IR spectra of the original tungsten disulfide and mechanocomposites (4 and 8 h) 1 – initial tungsten disulfide; 2 – mechanocomposite after 4 h; 3 – mechanocomposite after 8 h
Рис. 3. Область ИК-спектров исходного дисульфида вольфрама и механокомпози- тов (4 и 8 ч) 1 – исходный дисульфид вольфрама; 2 – механокомпозит после 4 ч; 3 – механокомпо- зит после 8 ч

Fig. 3 shows the IR spectra of the obtained mechanocomposites and the original tungsten disulfide. Due to the superposition of some peaks on each other there is a broadening of peaks in the regions of $450-750\text{ cm}^{-1}$. The peaks of the broad absorption band at 576 cm^{-1} , 613 cm^{-1} as well as the kink in the region of $625-655\text{ cm}^{-1}$ can be attributed to the valence vibrations of the W-O-W functional groups with oxygen positions at the edges and/or between the tungsten atoms [15-17]. In addition, based on literature data in the region of this broad absorption band there should be peaks of valence vibrations of the functional group W-S [18]. Also in the IR spectra of pure WS_2 and mechanocomposites, the peaks at 1613 and 3125 cm^{-1} and the kink at 1401 cm^{-1} are associated with valence and strain vibrations of the W-S functional group. The peak in the region of 1002 cm^{-1} can be attributed to the valence vibrations of W=O. The symmetric valence vibrations of W-O-W groups are characterized by a prominent peak at $887, 850\text{ cm}^{-1}$. At 1062 cm^{-1} , a peak associated with the strain vibrations of W-OH is observed. In addition to the above peaks, it should be noted that outside the enhanced region of the IR spectrum, peaks at 1627 and 3200 cm^{-1} are also present, related to the strain and valence vibrations of the -OH group of water, respectively. No changes in the number and positions of absorption bands are also observed. The differences between the IR spectra were found to be in the intensity of the peaks. The obtained data can only demonstrate the change in the concentration of compounds with the corresponding functional groups [19-21]. Based on the

above, the functional group data obtained by IR spectroscopy method does not provide specific and clear information about the difference of the obtained objects. This may indicate an insignificant difference in the composition of the objects due to the lack of possibility of formation under these conditions of compounds containing different functional groups from those described above.

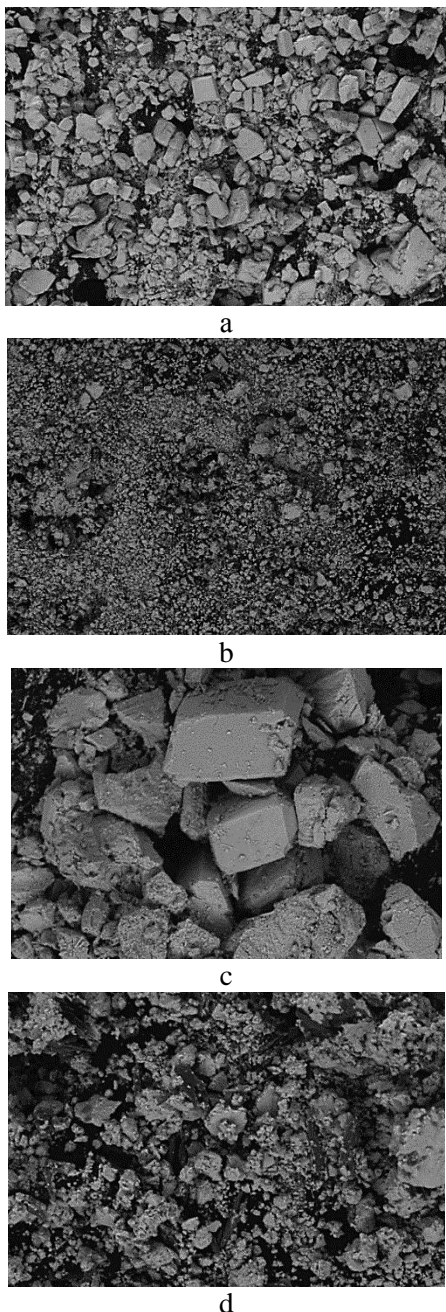


Fig. 4. Micrographs of the original tungsten disulfide (a, c) and the resulting mechanocomposite M-2 (b, d), taken in a scanning electron microscope at a resolution of 200 and 50 μm , respectively
 Рис. 4. Микрофотографии исходного дисульфида вольфрама (a, c) и полученного механокомпозиата М-2 (b, d), сделанные в сканирующем электронном микроскопе при разрешении 200 и 50 мкм, соответственно

In Fig. 4a shows a micrograph of tungsten disulfide powder. 4d particles with

Compared to SEM images of the original tungsten disulfide (Fig. 4c), loose bulk particles with asymmetric irregular shape with inclusions of smaller light particles are observed in sample M-2 (Fig. 4d). The average particle size is 10 μm and the light-colored particles are about 1 μm . The small light colored areas are tungsten trioxide particles and the asymmetrical irregularly shaped particles are tungsten disulfide particles. Tungsten trioxide particles are observed to stick together.

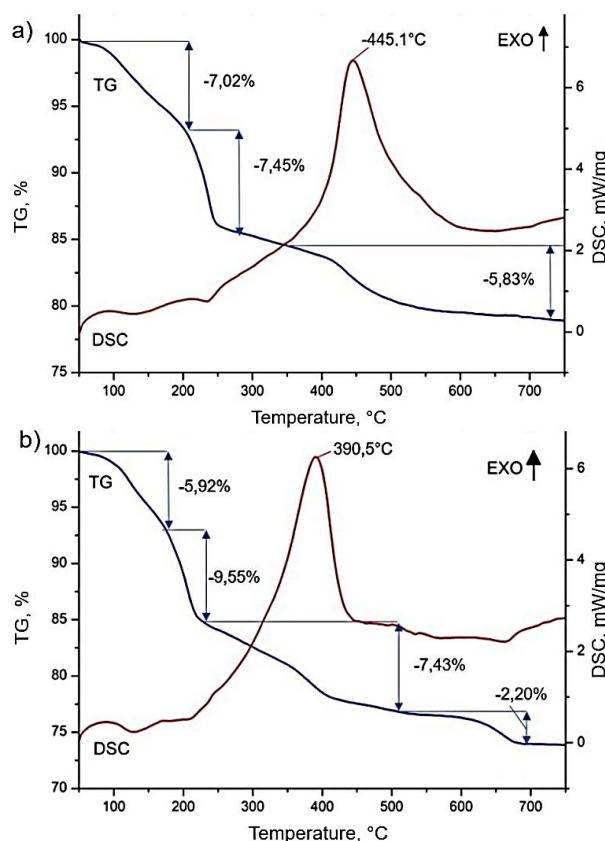


Fig. 5. TG and DSC thermal decomposition curves of tungsten disulfide (a) and mechanocomposite (b)

Рис. 5. ТГ и ДСК кривые термического разложения дисульфида вольфрама (a) и механокомпозиата (b)

The thermal studies demonstrate that compared to the original molybdenum disulfide, the mechanocomposite obtained in the process of mechanical activation has different thermal properties. Thermogravimetric curve (TG) analysis shows that there are four stages of mass loss process in the mechanocomposite, and the final mass loss of the mechanocomposite is higher compared to the disulfide, 25.1% and 20.3%, respectively. Synchronous thermal analysis (STA) of the initial tungsten disulfide and the obtained mechanocomposite was also carried out. The first mass

loss in the region of 180–210 °C can be attributed to the removal of chemically sorbed water. The second loss at 390 °C and 445 °C, is attributed to the partial oxidation of tungsten disulfide to tungsten trioxide. According to literature sources [22–28] the oxidation process of tungsten disulfide to tungsten trioxide is confirmed by the presence of a strong exothermic peak at 445 °C and a weight loss of 5.8%, which is close to the theoretical expected weight loss during the oxidation of tungsten disulfide to tungsten trioxide (–6.4%). In Fig. 5b, this peak is shifted to the left by about 50 °C, which may additionally indicate partial oxidation of tungsten disulfide. This may be due to the fact that less energy is required for a compound whose surface has already been partially oxidized. It is noteworthy that at temperatures above 600 °C no further weight loss is observed for tungsten disulfide, indicating complete oxidation of WS₂. These data are in full agreement with the disappearance of the characteristic peak of WS₂ in the XRD spectra corresponding to the annealing temperature of 600 °C. At the same time in the mechanocomposite there is a mass loss in the high-temperature region in the region from 620 to 700 °C, which is apparently related to the endothermic effect associated with the process of partial sublimation of surface oxide structures.

CONCLUSIONS

Thus, a number of mechanocomposites were synthesised in the course of the work. The obtained results indicate that at mechanoactivation more than 4 h oxidation of tungsten disulfide to tungsten oxides, mainly to tungsten trioxide begins. The oxidation process occurs at the stage of unloading the sample from the milling cup with argon, after contact of me-

chanically activated particles on the outer surface with air oxygen. According to XRD data, it can be concluded that mechanoactivation for 8 h is the most optimal. At the same time, a regular reduction in the intensity of tungsten disulfide reflexes is confirmed by the results of thermal analysis. In the case of surfactant addition to the system, it was found that the addition of any surfactant by nature (water, ethanol and hexane, hexadecane as an example) favours to obtain mechanocomposites with the required structure. Analysis of IR spectroscopy data did not give significant results. SEM data also show a decrease in the particle size and a change in their shapes, from which it follows that mechanical activation increases the specific surface area of the obtained mechanocomposites relative to the original powders.

ACKNOWLEDGMENTS AND FUNDING

The work was carried out with the financial support of the Russian Science Foundation, project No. 24-29-00582.

The authors gratefully acknowledge to the Center for Collective Use "Tomsk Scientific Center of SB RAS".

The authors declare the absence a conflict of interest warranting disclosure in this article.

Работа выполнена при финансовой поддержке РФФ, проект № 24-29-00582.

Авторы выражают благодарность Томскому региональному центру коллективного пользования ТИЦ СО РАН.

Авторы заявляют об отсутствии конфликта интересов, требующего раскрытия в данной статье.

ЛИТЕРАТУРА

1. **Choi W.** Recent Development of Two-Dimensional Transition Metal Dichalcogenides and Their Applications. *Mater. Today*. 2017. V. 20. P. 116–130. DOI: 10.1016/j.matod.2016.10.002.
2. **Tehrani M.** Synthesis of WS₂ nanostructures from the reaction of WO₃ with CS₂ and mechanical characterization of WS₂ nanotube composites. *Nanotechnology*. 2011. V. 22. N 28. P. 285714. DOI: 10.1088/0957-4484/22/28/285714.
3. **Zhu Y.** Shock-absorbing and failure mechanisms of WS₂ and MoS₂ nanoparticles with fullerene-like structures under shock wave pressure. *J. Am. Chem. Soc.* 2005. V. 127. P. 16263–16272. DOI: 10.1021/ja054715j.
4. **Singh R.** Ultrasmall Ni-Promoted WS₂ Nanocatalyst with Enhanced Number of Edge Atoms for Hydrodesulfurization. *Energy Fuels*. 2020. V. 34. N 1. P. 749–757. DOI: 10.1021/acs.energyfuels.9b03305.
5. **Yin C.** Effect of sulfidation process on catalytic performance over unsupported Ni-Mo-W hydrotreating catalysts. *Korean J. Chem. Eng.* 2017. V. 34. P. 1004–1012. DOI: 10.1007/s11814-017-0016-2.

REFERENCES

1. **Choi W.** Recent Development of Two-Dimensional Transition Metal Dichalcogenides and Their Applications. *Mater. Today*. 2017. V. 20. P. 116–130. DOI: 10.1016/j.matod.2016.10.002.
2. **Tehrani M.** Synthesis of WS₂ nanostructures from the reaction of WO₃ with CS₂ and mechanical characterization of WS₂ nanotube composites. *Nanotechnology*. 2011. V. 22. N 28. P. 285714. DOI: 10.1088/0957-4484/22/28/285714.
3. **Zhu Y.** Shock-absorbing and failure mechanisms of WS₂ and MoS₂ nanoparticles with fullerene-like structures under shock wave pressure. *J. Am. Chem. Soc.* 2005. V. 127. P. 16263–16272. DOI: 10.1021/ja054715j.
4. **Singh R.** Ultrasmall Ni-Promoted WS₂ Nanocatalyst with Enhanced Number of Edge Atoms for Hydrodesulfurization. *Energy Fuels*. 2020. V. 34. N 1. P. 749–757. DOI: 10.1021/acs.energyfuels.9b03305.
5. **Yin C.** Effect of sulfidation process on catalytic performance over unsupported Ni-Mo-W hydrotreating catalysts. *Korean J. Chem. Eng.* 2017. V. 34. P. 1004–1012. DOI: 10.1007/s11814-017-0016-2.

6. **Yang L.** Synergistic WO₃·2H₂O Nanoplates/WS₂ Hybrid Catalysts for High Efficiency Hydrogen Evolution. *ACS Appl. Mater. Interfaces*. 2016. V. 8. N 22. P. 13966–13972. DOI: 10.1021/acsami.6b04045.
7. **Курникова А.А., Румянцев Р.Н., Афиневский А.В., Борисова Т.Н., Севергина Е.С., Гордина Н.Е.** Мягкий механохимический синтез CuO/ZnO/Al₂O₃ катализатора для процесса получения метанола. *Изв. вузов. Химия и хим. технология*. 2024. Т. 67. Вып. 2. С. 21-29. DOI: 10.6060/ivkkt.20246702.6866.
8. **Лысенко Е.Н., Суржиков А.П., Власов В.А., Николаев Е.В., Минина Ю.С., Шевелева Е.А.** Влияние механической активации реагентов на синтез Li-Sm феррита. *Изв. вузов. Химия и хим. технология*. 2024. Т. 67. Вып. 3. С. 63-72. DOI: 10.6060/ivkkt.20246703.6931.
9. **Бакланова О. Н., Лавренов А.В., Василевич А.В.** Влияние механической активации на свойства носителей и катализаторов нефтепереработки. *Росс. хим. журн.* 2019. Т. 62. Вып. 1-2. С. 131-140. DOI: 10.6060/rj.2018621-2.11.
10. **Озолин А.В., Соколов Е.Г.** Влияние механической активации порошка вольфрама на структуру и свойства спеченного материала Sn-Cu-Co-W. *Обработка металлов: технология, оборудование, инструменты*. 2022. Т. 24. № 1. С. 48-60. DOI: 10.17212/1994-6309-2022-24.1-48-60.
11. **Акимов Ал.С., Жиров Н.А., Барбашин Я.Е., Герасимов Е.Ю., Акимов А.С.** Синтез и свойства систем на основе Ni- и изополимолибдат-содержащих соединений и метастабильных оксидов алюминия. *Изв. вузов. Химия и хим. технология*. 2023. Т. 66. Вып. 11. С. 85-91. DOI: 10.6060/ivkkt.20236611.16t.
12. **Tang H.** Effects of Defect and Temperature on the Mechanical Performance of WS₂: A Multiscale Analysis. *J. Phys. Chem. C*. 2021. V. 125. N 4. P. 2680–2690. DOI: 10.1021/acs.jpcc.0c09897.
13. **Falin A.** Properties of atomically thin tungsten dichalcogenides: WS₂, WSe₂, and WTe₂. *ACS Nano*. 2021. V. 15. N 2. P. 2600–2610. DOI: 10.1021/acsnano.0c07430.
14. **Zong L.** Hydrogels with WS₂ Nanosheets for Biomimetic Cellular Structures and Steerable Prompt Deformation. *ACS Appl. Mater. Interfaces*. 2017. V. 9. N 37. P. 32280–32289. DOI: 10.1021/acsami.7b10348.
15. **Cao S.** The WO₃/WS₂ nanostructures: Preparation, characterization and optical absorption properties. *Physica E: Low-Dimensional Syst. Nanostruct.* 2016. V. 81. P. 235–239. DOI: 10.1016/j.physe.2016.03.027.
16. **Shen Z.** Carbon-coated three-dimensional WS₂ film consisting of WO₃@WS₂ core-shell blocks and layered WS₂ nanostructures as counter electrodes for efficient dye-sensitized solar cells. *Electrochim. Acta*. 2018. V. 266. P. 130–138. DOI: 10.1016/j.electacta.2018.02.009.
17. **Zheng B.** WO₃-WS₂ Vertical Bilayer Heterostructures with High Photoluminescence Quantum Yield. *J. Am. Chem. Soc.* 2019. V. 141. P. 11754–11758. DOI: 10.1021/jacs.9b03453.
18. **Singh S.** Tungsten disulfide (WS₂) nanosheets: synthesis, characterization, adsorption studies and application for remediation of groundwater samples with high prevalence of uranium from Faridkot district of SW-Punjab. *J. Radioanalyt. Nuclear Chem.* 2021. V. 330. P. 1425–1436. DOI: 10.1007/s10967-021-07939-x.
19. **Yin W.** Synthesis of tungsten disulfide quantum dots for high-performance supercapacitor electrodes. *J. Alloys Compd.* 2019. V. 786. P. 764–769. DOI: 10.1016/j.jallcom.2019.02.030.
6. **Yang L.** Synergistic WO₃·2H₂O Nanoplates/WS₂ Hybrid Catalysts for High Efficiency Hydrogen Evolution. *ACS Appl. Mater. Interfaces*. 2016. V. 8. N 22. P. 13966–13972. DOI: 10.1021/acsami.6b04045.
7. **Kournikova A.A., Rumyantsev R.N., Afineevsky A.V., Borisova T.N., Severgina E.S., Gordina N.E.** Soft mechanochemical synthesis of CuO/ZnO/Al₂O₃ catalyst for methanol production. *ChemChemTech [Izv. Vyssh. Uchebn. Zaved. Khim. Khim. Tekhnol.]*. 2024. V. 67. N 2. P. 21-29 (in Russian). DOI: 10.6060/ivkkt.20246702.6866.
8. **Lysenko E.N., Surzhikov A.P., Vlasov V.A., Nikolaev E.V., Minina Yu.S., Sheveleva E.A.** Effect of mechanical activation of reagents on synthesis of Li-Sm ferrite. *ChemChemTech [Izv. Vyssh. Uchebn. Zaved. Khim. Khim. Tekhnol.]*. 2024. V. 67. N 3. P. 63-72. DOI: 10.6060/ivkkt.20246703.6931.
9. **Baklanova O. N., Lavrenov A.V., Vasilevich A.V.** The influence of mechanical activation on the properties of oil refining carriers and catalysts. *Ross. Khim. Zhurn.* 2019. V. 62. N 1-2. P. 131-140 (in Russian). DOI: 10.6060/rj.2018621-2.11.
10. **Ozolin A.V., Sokolov E.G.** The influence of mechanical activation of tungsten powder on the structure and properties of the sintered material Sn-Cu-Co-W. *Obrabotka metallov: Tekhnologiya, Oborudovanie, Instrumenty*. 2022. V. 24. N 1. P. 48-60 (in Russian). DOI: 10.17212/1994-6309-2022-24.1-48-60.
11. **Akimov Al.S., Zhiron N.A., Barbashin Ya.E., Gerasimov E.Yu., Akimov A.S.** Synthesis and properties of systems based on Ni- and isopolymolybdate-containing compounds and metastable aluminum oxides. *ChemChemTech [Izv. Vyssh. Uchebn. Zaved. Khim. Khim. Tekhnol.]*. 2023. V. 66. N 11. P. 85-91. DOI: 10.6060/ivkkt.20236611.16t.
12. **Tang H.** Effects of Defect and Temperature on the Mechanical Performance of WS₂: A Multiscale Analysis. *J. Phys. Chem. C*. 2021. V. 125. N 4. P. 2680–2690. DOI: 10.1021/acs.jpcc.0c09897.
13. **Falin A.** Properties of atomically thin tungsten dichalcogenides: WS₂, WSe₂, and WTe₂. *ACS Nano*. 2021. V. 15. N 2. P. 2600–2610. DOI: 10.1021/acsnano.0c07430.
14. **Zong L.** Hydrogels with WS₂ Nanosheets for Biomimetic Cellular Structures and Steerable Prompt Deformation. *ACS Appl. Mater. Interfaces*. 2017. V. 9. N 37. P. 32280–32289. DOI: 10.1021/acsami.7b10348.
15. **Cao S.** The WO₃/WS₂ nanostructures: Preparation, characterization and optical absorption properties. *Physica E: Low-Dimensional Syst. Nanostruct.* 2016. V. 81. P. 235–239. DOI: 10.1016/j.physe.2016.03.027.
16. **Shen Z.** Carbon-coated three-dimensional WS₂ film consisting of WO₃@WS₂ core-shell blocks and layered WS₂ nanostructures as counter electrodes for efficient dye-sensitized solar cells. *Electrochim. Acta*. 2018. V. 266. P. 130–138. DOI: 10.1016/j.electacta.2018.02.009.
17. **Zheng B.** WO₃-WS₂ Vertical Bilayer Heterostructures with High Photoluminescence Quantum Yield. *J. Am. Chem. Soc.* 2019. V. 141. P. 11754–11758. DOI: 10.1021/jacs.9b03453.
18. **Singh S.** Tungsten disulfide (WS₂) nanosheets: synthesis, characterization, adsorption studies and application for remediation of groundwater samples with high prevalence of uranium from Faridkot district of SW-Punjab. *J. Radioanalyt. Nuclear Chem.* 2021. V. 330. P. 1425–1436. DOI: 10.1007/s10967-021-07939-x.
19. **Yin W.** Synthesis of tungsten disulfide quantum dots for high-performance supercapacitor electrodes. *J. Alloys Compd.* 2019. V. 786. P. 764–769. DOI: 10.1016/j.jallcom.2019.02.030.

20. **Hazarika S.** Inorganic fullerene-type WS₂ nanoparticles: processing, characterization and its photocatalytic performance on malachite green. *Appl. Phys. A*. 2017. V. 123. N 5. DOI: 10.1007/s00339-017-0965-7.
21. **Liu N.** Synthesis of functional hollow WS₂ particles with large surface area for Near-Infrared (NIR) triggered drug delivery. *J. Alloys Compd.* 2021. V. 875. P. 1-8. DOI: 10.1016/j.jallcom.2021.160034.
22. **Garg M.** Lysine-functionalized tungsten disulfide quantum dots as artificial enzyme mimics for oxidative stress biomarker sensing. *ACS Omega*. 2020. V. 5. N. 4. P. 1927-1937. DOI: 10.1021/acsomega.9b03655.
23. **Nishiyama K.** Solid state tungsten oxide hydrate/tin oxide hydrate electrochromic device prepared by electrochemical reactions. *AIP Adv.* 2017. V. 7. N 3. P. 035004. DOI: 10.1063/1.4977963.
24. **Sun H.** Lattice-water-induced acid sites in tungsten oxide hydrate for catalyzing fructose dehydration. *Catal. Commun.* 2021. V. 149. P. 106254. DOI: 10.1016/j.catcom.2020.106254.
25. **Wu C.-M.** Recent Advances in Tungsten-Oxide-Based Materials and Their Applications. *Front. Mater.* 2019. V. 6. P. 1-17. DOI: 10.3389/fmats.2019.00049.
26. **Zhang X.** A facile synthesis and characterization of graphene-like WS₂ nanosheets. *Mater. Lett.* 2015. V. 159. P. 399-402. DOI: 10.1016/j.matlet.2015.07.044.
27. **Fan Y.** Synthesis, characterization and electrostatic properties of WS₂ nanostructures. *AIP Adv.* 2014. V. 4. N 5. P. 057105. DOI: 10.1063/1.4875915.
28. **Kang K.** The growth scale and kinetics of WS₂ monolayers under varying H₂ concentration. *Sci. Rep.* 2015. V. 5. P. 1-9. DOI: 10.1038/srep13205.
20. **Hazarika S.** Inorganic fullerene-type WS₂ nanoparticles: processing, characterization and its photocatalytic performance on malachite green. *Appl. Phys. A*. 2017. V. 123. N 5. DOI: 10.1007/s00339-017-0965-7.
21. **Liu N.** Synthesis of functional hollow WS₂ particles with large surface area for Near-Infrared (NIR) triggered drug delivery. *J. Alloys Compd.* 2021. V. 875. P. 1-8. DOI: 10.1016/j.jallcom.2021.160034.
22. **Garg M.** Lysine-functionalized tungsten disulfide quantum dots as artificial enzyme mimics for oxidative stress biomarker sensing. *ACS Omega*. 2020. V. 5. N. 4. P. 1927-1937. DOI: 10.1021/acsomega.9b03655.
23. **Nishiyama K.** Solid state tungsten oxide hydrate/tin oxide hydrate electrochromic device prepared by electrochemical reactions. *AIP Adv.* 2017. V. 7. N 3. P. 035004. DOI: 10.1063/1.4977963.
24. **Sun H.** Lattice-water-induced acid sites in tungsten oxide hydrate for catalyzing fructose dehydration. *Catal. Commun.* 2021. V. 149. P. 106254. DOI: 10.1016/j.catcom.2020.106254.
25. **Wu C.-M.** Recent Advances in Tungsten-Oxide-Based Materials and Their Applications. *Front. Mater.* 2019. V. 6. P. 1-17. DOI: 10.3389/fmats.2019.00049.
26. **Zhang X.** A facile synthesis and characterization of graphene-like WS₂ nanosheets. *Mater. Lett.* 2015. V. 159. P. 399-402. DOI: 10.1016/j.matlet.2015.07.044.
27. **Fan Y.** Synthesis, characterization and electrostatic properties of WS₂ nanostructures. *AIP Adv.* 2014. V. 4. N 5. P. 057105. DOI: 10.1063/1.4875915.
28. **Kang K.** The growth scale and kinetics of WS₂ monolayers under varying H₂ concentration. *Sci. Rep.* 2015. V. 5. P. 1-9. DOI: 10.1038/srep13205.

Поступила в редакцию 29.02.2024

Принята к опубликованию 14.05.2024

Received 29.02.2024

Accepted 14.05.2024